Chapter 4

First missense mutation in the SOST gene causing sclerosteosis by loss of sclerostin function

E. Piters, C. Culha,
M. Moester, R. van Bezooijen,
D. Adriaensen, T. Mueller,
S. Weidauer, K. Jennes,
F. de Freitas, C. Löwik,
J.P. Timmermans, W. Van Hul,
S. Papapoulos

Hum Mutat. 2010 Jul;31(7):E1526-43

Abstract

Sclerosteosis is a rare bone dysplasia characterized by greatly increased bone mass, especially of the long bones and the skull. Patients are tall, show facial asymmetry and often have syndactyly. Clinical complications are due to entrapment of cranial nerves. The disease is thought to be due to loss-of-function mutations in the *SOST* gene. The *SOST* gene product, sclerostin, is secreted by osteocytes and transported to the bone surface where it inhibits osteoblastic bone formation by antagonizing Wnt signaling. In a small Turkish family with sclerosteosis, we identified a missense mutation (c.499T>C; p.Cys167Arg) in exon 2 of the *SOST* gene. This type of mutation has not been previously reported and using different functional approaches, we show that it has a devastating effect on the biological function of sclerostin. The affected cysteine is the last cysteine residue of the cystine-knot motif and loss of this residue leads to retention of the mutant protein in the ER, possibly as a consequence of impaired folding. Together with a significant reduced ability to bind to LRP5 and inhibit Wnt signaling, the p.Cys167Arg mutation leads to a complete loss of function of sclerostin and thus to the characteristic sclerosteosis phenotype.

Introduction

Bone mineral density (BMD) in humans is a quantitative trait determined to a great extent by genetic factors [1, 2]. The involvement of genes has been clearly demonstrated in patients with sclerosing bone dysplasias, a heterogeneous group of 40 different monogenetic diseases associated with increased BMD. One subgroup comprises the craniotubular hyperostoses, mainly characterized by increased cortical thickness of the long bones and the skull [3, 4]. Sclerosteosis (SCL; MIM# 269500) and Van Buchem disease (VBD; MIM# 239100) are two closely related, rare craniotubular hyperostoses with an autosomal recessive mode of inheritance.

Patients with SCL show progressive bone overgrowth and thickening, especially of the skull, the mandible and the tubular bones. Patients are tall and have facial distortion due to enlargement of the mandible and forehead. Entrapment of cranial nerves often results in facial nerve palsy, hearing loss, and loss of smell. Calvarial overgrowth leads to elevated intracranial pressure causing headache and occasionally sudden death. The majority of patients with SCL have some degree of hand malformations, mainly syndactyly. These features are not present in patients with VBD and together with tall stature, may allow the clinical differentiation of the two conditions [5-8]. Sclerosteosis has a high prevalence in the Afrikaner population in South-Africa. In addition, it has been reported in isolated individuals or families from Spain, Brazil, the USA, Germany, Japan and Senegal [9-16]. Apart from an isolated family in Scotland, patients with VBD are Dutch, originating from an isolated community in The Netherlands [17]. Because the Africaner population is of Dutch origin, it was assumed that SCL and VBD were caused by the same genetic defect. The mapping of SCL to locus 17q12-21, the region that was also shown to contain the gene responsible for VBD, further supported this hypothesis [18, 19]. However, genetic analysis revealed that the two conditions have a different genetic defect. Through positional cloning, Balemans *et al.* identified two homozygous nonsense mutations (c.372G>A (p.Trp124X); c.376C>T (p.Arg126X)) in a Brazilian and an American SCL family, respectively, and a splice site mutation (c.220+3A>T) in a Senegalese patient with SCL in the previously unknown *SOST* gene (MIM# 605740) [20]. Simultaneously, Brunkow *et al.* identified a homozygous nonsense mutation (c.70C>T (p.Gln24X)) in affected individuals from South Africa. The nonsense mutations lead to premature termination of the protein, while the c.220+3A>T

mutation was shown to alter splicing of the *SOST* gene [21]. In 2005, another splice-site mutation (c.220+1G>C) in the *SOST* gene was reported in two affected siblings of German origin, putatively disease-causing in the same way as the c.220+3A>T mutation [22]. In the Dutch patients diagnosed with VBD no *SOST* mutation was present, but a 52kb deletion downstream of the *SOST* gene was identified. This deleted region harbours an enhancer element that drives the expression of the *SOST* gene explaining the similarities between the two conditions [23, 24]. All of the reported mutations in *SOST* as well as the deletion found in patients with VBD, result in the absence of expression of the *SOST* gene product sclerostin by osteocytes [25, 26].

In patients with SCL and VBD, the increase in BMD is due to increased bone formation [14, 26-28]. In addition, mouse models with deletion or overexpression of the *SOST* gene as well as *in vitro* studies of osteoblast proliferation and differentiation, matrix mineralization and apoptosis demonstrated that sclerostin has an inhibitory action on bone formation [26, 29-32]. Although the precise molecular mechanism of action of sclerostin still needs to be elucidated, it has been shown that it antagonizes Wingless-Int (Wnt) signaling and binds directly to the first two ß-propellers of low density lipoprotein receptor related protein (LRP) 5, but does not compete with the binding of Wnt proteins to LRP5/6 receptors [31, 33, 34]. LRP5 is required for the transduction of Wnt signals and the first ß-propeller domain of LRP5 is known to harbour mutations causing a High Bone Mass (HBM) phenotype [35-37]. This condition is also classified among the craniotubular hyperostoses and has an autosomal dominant mode of inheritance. For all these LRP5 mutants, binding to sclerostin was found to be impaired [38-40]. Furthermore, just like in patients with VBD and SCL, the bone thickening is most obvious at the long bones and the mandible, favouring a shared pathogenesis with SCL and VBD [41].

In this paper, we describe the genetic analysis of a patient with SCL and her relatives resulting in the identification of the first missense mutation in the *SOST* gene. This mutation results in the exchange of a cysteine residue of the cystine-knot motif of sclerostin for a non-cysteine amino acid, a defect that leads to a complete loss of function of sclerostin due to retention of the mutated protein in the ER.

Materials and methods

Mutation analysis

We analysed both exons of the *SOST* gene as well as exon 2, 3 and 4 of the LRP5 gene that comprise the first ß-propeller domain of the LRP5 protein, in which all mutations causing craniotubular hyperostoses cluster. In a first step, amplification was performed by GoTaq DNA polymerase-mediated PCR (Promega Corporation, Madison, Wisconsin, USA). Primers used to generate fragments containing the exons and its exon-intron boundaries of the *SOST* gene were: forward primer (FW) 5'-AGAATTCTCTCCTCCACCC-3' and reverse primer (R) 5'-GTGCTACTGGAAGGTGGC-3' for exon 1 and FW 5'-CCCCTGCCCT GGGTTGC-3' and R 5'-CTTTCCACCAGCTCTAGAGC-3' for exon 2. For LRP5, exon 2 was amplified using FW 5'-AACTTCCTGACAACGCCTTAGG-3' and R 5'-TGCCATTGAGGTTGGCCACC-3', exon 3 using FW 5'-CGATGGGTGAGA TTTTAGGG-3' and R 5'-TGACGCTGTTCCAAGTTCTG-3', and exon 4 with FW 5'-GGGTCAGCAGCAATGACTGTCGG-3' and R 5'-CCAGAGCATGGGCTT CTGCAGG-3'. Amplified fragments were verified by agarose gel electrophoresis and compared with the Generuler 100 bp Plus DNA Ladder (Fermentas International Inc, Ontario, Canada). Primers and unincorporated deoxyribonucleotide triphosphates (dNTPs) were removed using exonuclease I (New England Biolabs, Inc, Ipswich, Massachusetts, USA) and calf intestine alkaline phosphatase (CIAP, Roche Applied Science, Hoffmann–La Roche AG, Basel, Switzerland). Sequencing was carried out directly on purified fragments with the ABI 310 Genetic Analyser (Applied Biosystems, Foster City, California, USA), using ABI Prism BigDye Terminator Cycle Sequencing Ready Reaction Kit, version 1.1 (Applied Biosystems, Foster City, California, USA). The BigDye XTerminator Purification Kit was used as purification method for DNA sequencing to remove unincorporated BigDye terminators.

Expression constructs and *in vitro* mutagenesis

Alignment of the human sclerostin protein sequence (GenBank RefSeq NM_025237.2) and its homologue in mouse (GenBank RefSeq NM_024449.5) showed that c.493T>C (p.Cys165Arg) in mouse corresponds with c.499T>C (p.Cys167Arg) in human (nucleotide numbering refers to the cDNA RefSeq

using the A of the ATG translation initiation codon as nucleotide +1). Using the QuikChange Site-Directed Mutagenesis Kit (Stratagene, La Jolla, California), we introduced this mutation in a pcDNA3.1 plasmid that produces a secreted form of the WT mouse sclerostin with an HA tag at the amino terminus (WT m*Sost*-HA). This construct contains the following elements (5' to 3'): NheI site, IgG kappa light chain signal peptide sequence (QTHILLWVLLLWVQGSTGD), HA tag sequence (YPYDVPDYA), two linker peptide residues (GA), EcoRI site, m*Sost* lacking endogenous signal peptide, termination codon, and XhoI site. Following primers were used for *in vitro* mutagenesis: FW 5'CCTCGTGCAAGCGCAAGCGCC- 3' and R 5'-GGTGAGGCGCTTGCGCTTGCA-3'. The complete insert sequence was verified for the presence of the mutation and for the absence of PCR introduced errors, using FW 5'ACCGAGTTGGTGTGCTCC- 3' and R 5'-GCACAGCAGCTGCACCC-3' as primers for direct sequencing on plasmid DNA. Although the mouse *Sost* gene has high similarity with the human *SOST* gene in the affected region, a human *SOST* construct was also used and the p.Cys167Arg mutation was introduced by site-directed mutagenesis at Genscript, Piscataway, USA.

The expression construct mouse Wnt1-V5 was kindly provided by Bart Williams (Van Andel Research Institute, USA) and Mesdc2 by Bernadette Holdener (State University of New York, USA). Both untagged full-length human WT-LRP5 and truncated human WT-LRP5 lacking the transmembrane and cytoplasmic domains but with a c-myc epitope at the carboxy-terminus were obtained from Matthew Warman (Howard Hughes Medical Institute, Orthopaedic Research Laboratories, USA). Bert Vogelstein (The Johns Hopkins University School of Medicine, USA) provided the Topflash Wnt reporter construct (pGL3-OT) while the BAT-luc Wnt reporter construct was provided by Stefano Piccolo (University of Padua School of Medicine, Italy). The Renilla luciferase constructs pRL-TK and pRL-SV40 were purchased from Promega Corporation.

Red fluorescent protein (RFP) fusion proteins for WT and MT mouse *Sost* were generated using the above described WT and MT m*Sost*-HA as a template. PCR amplification was performed to disrupt the termination codon and the complete region of interest was subcloned into a pTurboFP635-N vector (Evrogen JSC, Moscow, Russia) to obtain WT and MT m*Sost*-RFP, respectively. A vector encoding a termination codon in the m*Sost* gene served as a negative control (ter-m*Sost*-RFP).

Immunoblotting

The human embryonic kidney (HEK) cell line 293T obtained from Danny Huylebroeck (University of Leuven, Leuven, Belgium), was grown in DMEM (Gibco- Invitrogen Ltd, Paisley, UK) supplemented with FBS (10% v/v). Twenty-four hours prior to transfection, HEK293T cells were plated at 4 x 10^5 cells/well in 6-well plates (Greiner Bio-One, Kremsmünster, Austria). Cells were transiently transfected with either WT or MT m*Sost*-HA or empty pcDNA3.1 vector (500 ng/well) using FuGENE 6 (Roche Applied Science), according to the manufacturer's instructions. Twenty-four hours after transfection, the culture medium was changed to 1 ml serum-free DMEM and 48 h after transfection, conditioned medium (CM) was collected and cells were lysed with 500 µl radioimmune precipitation (RIPA) buffer per well (50 mM Tris-HCl pH 8.0; 150 mM NaCl; 1% NP-40; 0.5% Na-deoxycholate; 0.1% SDS; complete protease inhibitor cocktail tablet (Roche Applied Science); benzonase endonuclease (Merck, Darmstadt, Germany)). Total protein in cell lysates was quantified using a bicinchoninic acid (BCA) assay (Pierce, Illinois, USA) with the purpose of loading equal protein amounts on SDS-PAGE. CM and cell lysates were diluted in 5x SDS-PAGE loading buffer and subjected to reducing SDS-PAGE. After transfer to a PVDF membrane, sclerostin-HA was detected using a rabbit polyclonal HA antibody (1:2000; BD Biosciences, San Diego, CA). Equal protein loading for lysate fractions was verified with a mouse ß-actin antibody (1:5000; Sigma-Aldrich, St. Louis, MO). Secondary incubation was performed using a goat anti-rabbit IgG-HRP (1:10000; Biorad) and a sheep anti-mouse IgG-HRP (1:5000; Amersham Biosciences), respectively, for 2 h at room temperature. Chemiluminescence detection was carried out using the Enhanced Chemiluminescence (ECL) Western Blotting Substrate (Pierce) according to the manufacturer's instructions.

Electrochemiluminescence assay by Meso-Scale Discovery

HEK293T cells and Saos-2 human sarcoma cells (ATCC) were grown in DMEM supplemented with FBS (10% v/v). Twenty-four hours prior to transfection, HEK293T and Saos-2 cells were plated at 1.3 x 10^5 and 4.5 x 10^4 cells/well in 24-well plates (Greiner Bio-One), respectively. Cells were transfected with WT and MT constructs of both mouse and human *Sost*/*SOST* or a control plasmid (empty pcDNA3.1). After 24h, medium was replaced and after further incubation for 24 h, CM was collected

and cells were lysed with 250 µl Meso-Scale Discovery (MSD, Gaithersburg, MD, USA) lysis buffer per well (20 mM Tris-HCl pH 7.5; 150 mM NaCl; 1 mM EDTA; 1 mM EGTA; 1% Triton X-100; complete protease inhibitor cocktail tablet (Roche Applied Science); 10 mM NaF) or total RNA was isolated for RT-PCR analysis. Sclerostin levels in CM and cell lysates were determined using the 96-well MULTI-ARRAY® human sclerostin assay (MSD) according to the manufacturer's instructions and corrected for *SOST* mRNA expression as determined by RT-PCR analysis.

Co-localisation studies using confocal live cell imaging

HEK293T and Saos-2 cells were grown in DMEM supplemented with FBS (10% v/v). Twenty-four hours prior to transfection, cells were plated at low-density (0.5 x 10^5 cells/well) in 24-well plates (Greiner Bio-One). Both cell types were transfected with WT or MT m*Sost*-RFP plasmid DNA, or with the ter-m*Sost*-RFP as an empty control (200 ng). FuGENE 6 (Roche Applied Science) was used for transfection; FuGENE 6 reagent: DNA ratio was slightly higher for Saos-2 cells (4:1) than for HEK293T cells (6:1). Twenty-four hours after transfection, medium was removed and cells were rinsed with 1x Hanks balanced salt solution (HBSS) (Gibco Invitrogen Ltd). In addition, staining with a green fluorescent tracer for live-cell ER labeling (ER-Tracker™ Green (glibenclamide BODIPY® FL); Molecular Probes Invitrogen Ltd) was performed. Cells were incubated for 20 min at 37°C after adding 1 µM ER-Tracker™ Green staining solution. Subsequently, the staining solution was replaced by probe-free medium and cells were imaged using an inverted microscope (Zeiss Axiovert 200; Carl Zeiss, Jena, Germany) attached to a microlensenhanced dual spinning disk confocal system (UltraVIEW ERS, PerkinElmer, Seer Green, UK), equipped with a three-line (488, 568 and 647 nm) argon–krypton laser. Red fluorescent fusion proteins (excitation maximum (ex max): 553 nm; emission maximum (em max): 574 nm) were excited by the 568 nm line while the green ER stain (ex max: 504 nm; em max: 511 nm) was excited by the 488 nm line. Fluorescence was recorded using 527/55 nm and 615/70 nm band pass filters, respectively. Multicolor high-resolution time-lapse images (4 images/s) of the living cells were captured over a time period of 5 min. Data were analyzed by Volocity 5 software (Improvision, PerkinElmer).

Wnt activity reporter assays

Saos-2 cells were grown in DMEM supplemented with FBS (10% v/v). Twenty-four hours prior to transfection, cells were plated at 1.25 x 10^5 cells/well in 24-well plates and at 6.75 x 10^3 cells/well in 96-well plates (Greiner Bio-One) for stimulation with Wnt1-V5 and recombinant Wnt3A (rec Wnt3A), respectively. Cells were transfected using FuGENE 6 or FuGENE HD (Roche Applied Science), respectively, according to the manufacturer's instructions. For stimulation with Wnt1-V5 (100 ng/well), cells were co-transfected with Mesdc2 (20 ng/well), pGL3-OT reporter (100 ng/well) and untagged full length WT-LRP5 (20 ng/well) in the presence or absence of WT or MT m*Sost*-HA (40 ng/well). For stimulation with rec Wnt3A, cells were transfected with untagged full length WTLRP5 (40 ng/well) and BAT-luc (20 ng/well) and stimulated with 30 ng/ml rec Wnt3A, 24h after the transfection. When necessary, empty pcDNA3.1 vector was added to make the total DNA amount equal for all transfection experiments. The Renilla luciferase constructs pRL-TK and pRL-SV40 were co-transfected to correct for transfection efficiency of Wnt1-V5 and rec Wnt3A, respectively. Forty-eight hours after transfection, cells were lysed using 100 µl passive lysis buffer (Promega Corporation). Firefly and Renilla luciferase activity were measured using the dual-luciferase reporter assay system (Promega Corporation) according to manufacturer's instructions.

Co-immunoprecipitation

Conditioned media and cell lysates containing WT or MT-sclerostin-HA were obtained as described above. In case of LRP5, HEK293T cells were co-transfected with truncated human WT-LRP5-myc (1 µg) and, in equal amounts, Mesdc2. Proper expression of LRP5-myc protein in CM was evaluated by immunoblotting with c-myc antibodies (clone 9E10; Sigma-Aldrich; dilution 1:5000). Rabbit polyclonal HA antibody was used to verify the presence of WT and MT sclerostin-HA in CM or total cell lysates. Equal protein loading for lysate fractions was verified using ß-actin antibodies. Based on these results, sclerostin-containing CM or total cell lysates were diluted more in the co-immunoprecipitation (co-IP) reactions than LRP5-containing CM. Co-IP between sclerostin and LRP5 was carried out by mixing CM containing truncated WT-LRP5-myc with CM containing WT-sclerostin-HA or cell lysates containing MT-sclerostin-HA, respectively. For the co-

IP reactions, EZ-view™ Red Anti-HA affinity gel (Sigma-Aldrich) was pre-blocked for 1h with 3% BSA (Sigma-Aldrich) in 1x TBS buffer (pH7.8) at 4°C using a rotation shaker. Hundred µl of CM containing WT-sclerostin-HA or cell lysates containing MTsclerostin-HA was mixed with equivalent amounts of secreted LRP5 (total CM volume of 250 µl), together with 45 µl of pre-blocked EZ-view™ Red Anti-HA affinity gel. The final volume was adjusted to 1 ml with 1x TBS, and incubated for 4h at 4°C using a rotation shaker. To remove unbound proteins, the affinity gel was washed at 4°C in wash buffer (50 mM Tris-HCl pH7.5; 150 mM NaCl; 0.1% Triton-X100) for 5 min, and then pelleted. Protein complexes were eluted by resuspending the pellets in 1x PBS buffer containing 100 µg/ml HA-peptide (Sigma- Aldrich). After 15 min incubation at room temperature, supernatants were collected and stored for SDS-PAGE. To serve as a positive control for binding to the affinity column, IP was also performed by adding a comparable volume of CM containing WT-sclerostin-HA, or cell lysates containing MT-sclerostin-HA to the preblocked EZ- view™ Red Anti-HA affinity gel. In the same way, a comparable volume of CM containing truncated WT-LRP5myc not expressing the HA-tag, was used as a negative control for IP on an anti-HA affinity gel. Following transfer to PVDF, LRP5-myc and sclerostin-HA were incubated with anti-c-myc and anti-HA, respectively. Subsequently, LRP5-myc and ß-actin proteins were incubated with secondary anti-mouse IgG-HRP for 2h at room temperature; sclerostin-HA with a secondary goat anti-rabbit IgG-HRP. Chemiluminescence detection was carried as described above.

Statistical analysis

Data are expressed as mean values ± SD. Comparisons between two or more measurements for a single experiment were performed using a Student's t-test and one-way ANOVA, respectively. For a set of experiments, general linear model (GLM) was used. Values of $p<0.05$ were considered significant. In case of post hoc multiple comparisons, Bonferroni was used. All statistical tests were provided by the SPSS 15.0 software package (SPSS Inc.).

Modeling of MT sclerostin

Modeling of the effect of the mutation was based on the NMR structure of mouse sclerostin (PDB entry 2KD3). The coordinates comprising the residues Asn59 to

Arg167 of mouse sclerostin (corresponding to residues Asn61 to Arg169 of human sclerostin) were used for the analysis. After adapting the numbering to human sclerostin residue Cys167 was replaced by arginine using the protein modeling tools of the software package Quanta2006 (Accelrys Inc, San Diego). Due to the previous amino acid Cys167 being involved in a disulfide bond with residue Cys109 and the resulting steric clash with the large side chain of the Arg167 introduced, the side chain was manually reoriented such that the side chain of Arg167 pointed towards the solvent requiring changes in the backbone conformation of the lower part of the flexible loop (starting from residue Gly110). The structure was subsequently refined by energy minimization runs; only geometrical energy terms without any electrostatic contribution were employed. Analysis of the resulting structure of MT sclerostin showed comparable statistics for backbone torsion angle distribution and van der Waals contacts. To test whether the replacement of Cys167 into Arg167 influences the flexibility of the loop, which has been proposed to contain the binding epitope of sclerostin for LRP5, molecular dynamics (MD) simulation runs were performed with or without NMR distance restraints derived for WT mouse sclerostin. All dynamics simulations were done using the software package Quanta2006 and the force field CHARMM22 without electrostatic energy terms (Accelsrys Inc, San Diego), the non-bonded cut-off for van der Waals interactions was set to 10.5Å, the temperature of the bath was kept at 300K to allow for sufficient mobility of the atoms.

Results

Clinical description

A 28-year old Turkish woman from a consanguineous marriage was recognized with clinical features suggestive of SCL (Figure 1A) and HBM during investigation of a multinodular goitre. She suffered from recurrent facial nerve palsies at the ages of 9, 14 and 15 years, complained of severe headaches, and had bilateral mixed-type hearing loss and right visual loss. Her height was 190 cm, weight 76 kg and head circumference 66.5 cm. The skull and jaw were enlarged, and she had proptosis and high arched palate. No syndactyly or other hand malformations were observed. Skull radiographs showed thickening of the calvarium (Figure 1B-C), an enlarged mandible and a highly increased BMD (T-score: spine +10.6, femoral neck +9.6).

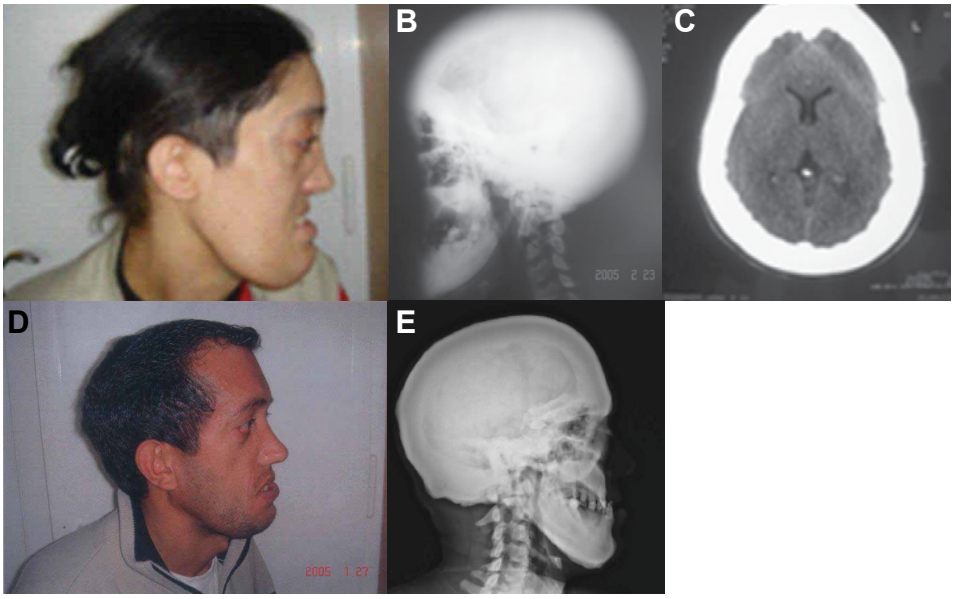

Figure 1. A) Lateral view of the female patient's face showing a marked mandibular prognathism. B) Plain radiograph of the skull (lateral view) showing uniform sclerosis of the calvaria, skull base and facial bones (particularly the mandible). C) Axial CT-scan of the brain showing marked thickening of the cranial vault. D) Lateral view of the face of the female's brother, who also shows a marked mandibular prognathism. E) Plain radiograph of the skull (lateral view) of the brother, showing uniform sclerosis of the skull and the mandible.

Endocrinological investigations revealed no abnormalities except for thyroid function compatible with subclinical hyperthyroidism. Her 35-year-old brother showed a similar phenotype with a rather uniform sclerosis of the skull, a thickened calvarium and an enlarged mandible, which can be noticed from the radiographs (Figure 1D-E). This patient also was of tall stature (190 cm), had a large head (head circumference: 66 cm) and a highly increased BMD (T-score: spine +9.8, femoral neck +7.3). Similar to his sister, he had no syndactyly or other hand malformations. Information on the presence of additional clinical symptoms was lacking. Other family members were phenotypically normal.

Mutation analysis

Because mutations in LRP5 and *SOST* are known to be causal for craniotubular hyperostoses, we evidently included both genes in the mutation screening of the patient. Direct sequencing of the LRP5 gene revealed no mutations in the coding region of the gene or in the exon-intron boundaries. Instead, we found a homozygous

c.499T>C (p.Cys167Arg) mutation in exon 2 of the *SOST* gene (nucleotide numbering refers to the cDNA RefSeq using the A of the ATG translation initiation codon as nucleotide +1) (data not shown). To investigate whether the mutation segregated with the disease, additional family members were recruited and sequenced. This resulted in the identification of the same homozygous missense mutation in an affected brother. Both unaffected parents and an unaffected sibling were found to be heterozygous carriers. Eighty unrelated healthy control individuals (160 chromosomes) from Turkish origin were checked for the presence of this mutation and all turned out to be negative.

Decreased intracellular and extracellular levels of MT sclerostin

Since sclerostin is a secreted protein, we initially tested the intra- and extracellular presence of the mutated protein by transient transfection of HEK293T cells with WT and MT mouse *Sost*-HA plasmids. Transfection with a negative control plasmid (empty pcDNA3.1) was also included. All transfection efficiencies were similar as measured by ß-galactosidase activity (data not shown). By immunoblotting, both WT and MT sclerostin were detected in the cell lysates, indicating that the MT protein was formed and recognized by the HA antibody. Moreover, the increased presence of MT sclerostin in the cell lysate suggested an upregulation of expression of the functionally inactive MT sclerostin. In CM, only WT sclerostin was present (Supplementary Figure 1A).

To further investigate the effect of the mutation on intra- and extracellular levels of sclerostin, a quantitative electrochemiluminescence assay was used to measure the concentration of WT and MT mouse sclerostin in HEK293T cells (Supplementary Figure 1B-C) and Saos-2 cells (data not shown). In addition, human *SOST* plasmids with or without the mutation were tested in both cell lines. After correction for *SOST* mRNA, both the intra- and extracellular levels of mouse and human MT sclerostin were lower than those of WT sclerostin. The levels of human sclerostin were consistently higher than those of mouse sclerostin, which may be due to differences in expression efficiency of the plasmids and/or the sensitivity of the assay to mouse and human sclerostin.

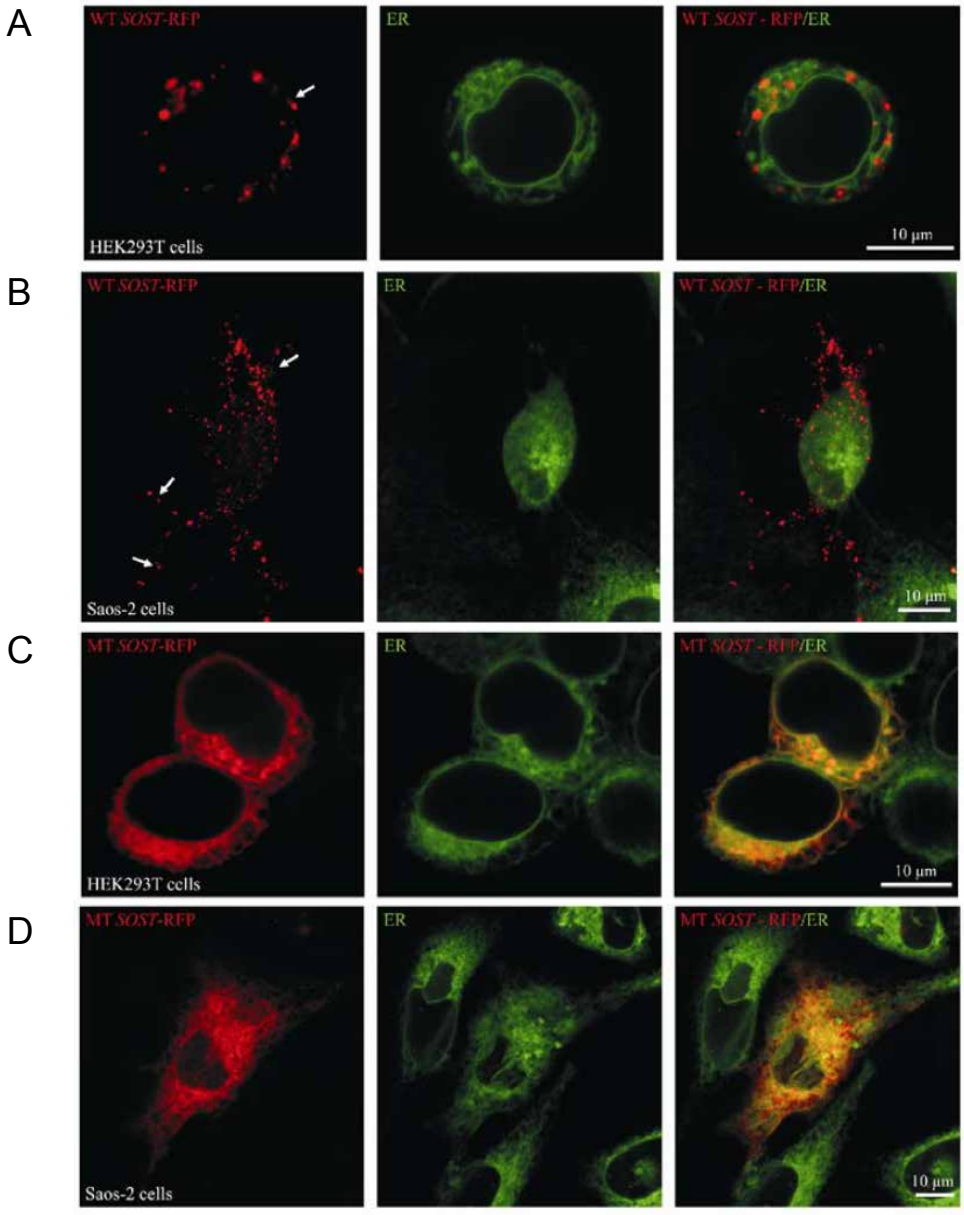

Figure 2. Retention of MT sclerostin in the ER. A-B. HEK293T (A) and Saos-2 cells (B) were transiently transfected with WT SOST-RFP plasmid to study the subcellular localization of WT mouse sclerostin (red channel). ER staining was performed using a green fluorescent ER tracker (green channel). Living cells were viewed using an UltraVIEW dual spinning disk confocal system. Arrows indicate the presence of WT sclerostin in variably sized granular cytoplasmic structures, preferentially in areas close to the cell membrane. The ER networks typically showed the highest density around the nucleus. Merging of the red and green channels clearly revealed that both labels are not co-localized. The latter was most obvious in the many cytoplasmic processes of Saos-2 cells. C-D. Similar to Figure 4 A-B, but now HEK293T (C) and Saos-2 cells (D) were transfected with MT SOST-RFP. The orange/yellow color in the merged channel images revealed a major co-localization of MT SOST protein with the ER tracker in both cell types. Scale bars are indicated.

Retention of MT sclerostin in the ER

As no previous intracellular localization studies had been reported for sclerostin, we hypothesized that, similar to other newly synthesized secreted proteins, it should be produced in the ER from where it is further targeted into the secretory pathway via the Golgi apparatus and cytoplasmic secretory granules. Mutations in proteins often lead to misfolding and subsequent retention in the ER [42]. To study the effect of the mutation on the subcellular localization of sclerostin in HEK293T and Saos-2 cells, we generated RFP fusion proteins for both WT and MT sclerostin, and the ER was visualized using a green fluorescent ER tracker. By confocal live-cell imaging, we found that the presence of WT sclerostin was concentrated in granular cytoplasmic structures, indicative of secretory granules (Figure 2A-B). The granular staining was most prominent in areas close to the cell membrane and hardly co-localized with the green fluorescent ER tracker, for which the staining was seen as a rather uniform network around the nucleus. The staining pattern of the MT sclerostin-RFP fusion protein was more diffuse and appeared to predominantly co-localize with the ER tracker (Figure 2C-D).

Decreased antagonistic activity of MT sclerostin

The effect of the mutation on the antagonistic capacity of sclerostin on Wnt signaling was tested in Saos-2 cells. Cells were transfected with a Wnt reporter construct and stimulated with either a Wnt1 expression plasmid or rec Wnt3a. Transfection of Wnt1 alone resulted in a 2-fold enhancement of Wnt signaling (Figure 3A). However, when the Wnt1 plasmid was co-transfected with an LRP5 expression plasmid, a 13-fold increase in Wnt signaling was observed. Wild type m*Sost* plasmid significantly inhibited Wnt1-stimulated Wnt signaling to almost 50% of its original level ($p= 0{,}007$), whereas the MT m*Sost* plasmid could only induce a non-significant 20% reduction. Stimulation with rec Wnt3a resulted in an almost 20-fold increase in Wnt signaling (Figure 3B). Both mouse and human WT *Sost*/*SOST* plasmids significantly inhibited Wnt signaling, and the human *SOST* plasmid seemed to be more potent. Both MT *Sost*/*SOST* plasmids did not inhibit rec Wnt3a-induced signaling.

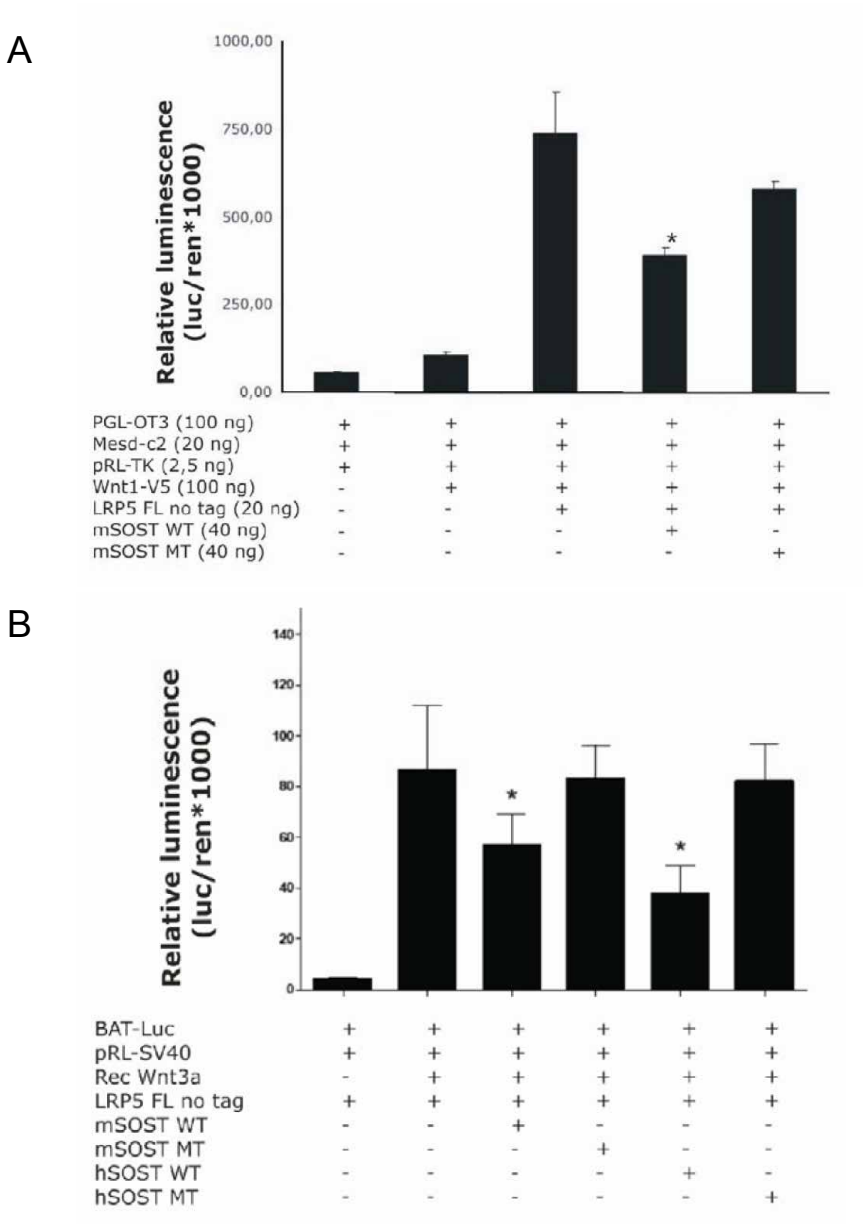

Figure 3. Decreased level of Wnt signal transduction both in the presence of human and mouse MT sclerostin. A) Saos-2 cells were transiently transfected with pGL3-OT, pRL-TK, Mesdc2, untagged full length WT-LRP5 in the presence or absence of Wnt1-V5. The antagonistic activity on Wnt signaling was evaluated by co-transfecting either WT or MT mSOST. Data were generated in three independent experiments, each performed in triplicate. Bars represent mean values ± SD. * $p<0.05$ cells transfected with WT mSOST compared to cells transfected without WT mSOST. B) Saos-2 cells were transfected with untagged full length WT-LRP5 and BAT-luc with or without mouse and human WT or MT SOST expression vectors and stimulated with rec Wnt3a 24h after transfection (n=8). Bars represent mean values ± SD. * $p<0.05$ cells transfected with mouse or human WT SOST compared to cells transfected without mouse or human WT SOST. All data were corrected for differences in transfection efficiency by co-transfection with constitutively active Renilla-luciferase expression plasmids.

Impaired binding of MT sclerostin to LRP5

Co-IP experiments were performed to evaluate the effect of the mutation on the ability of sclerostin to interact with LRP5. HEK293 cells were transfected with constructs either expressing truncated LRP5-myc (encoding only the extracellular part of the protein), WT-sclerostin-HA, or MT-sclerostin-HA. Figure 4A illustrates that truncated LRP5-myc and WT-sclerostin-HA were expressed in the CM, while MT-sclerostin-HA was found exclusively in the cell lysate (Figure 4A). Subsequently, CM of the truncated LRP5-myc transfected cells was mixed with either CM of WT-sclerostin-HA transfected cells or cell lysates of MT-sclerostin-HA transfected cells to determine binding between the extracellular part of LPR5 and WT- en MT-sclerostin. From the immune complexes, HA-tagged WT- and MT-sclerostin were precipitated using EZ-view™ Red Anti-HA affinity gel and immunoblotted with c-myc antibodies to demonstrate co-IP of truncated LRP5-myc with WT- or MT-sclerostin-HA. Truncated LRP5-myc was detected in precipitates that contained WT-sclerostin-HA, but not in precipitates that contained MT-sclerostin-HA, suggesting that the mutation in sclerostin resulted in a reduced affinity for LRP5 (Figure 4B). The immune complexes were also immunoblotted with anti-HA to demonstrate the presence of either WT- or MTsclerostin-HA in all samples (Figure 4B).

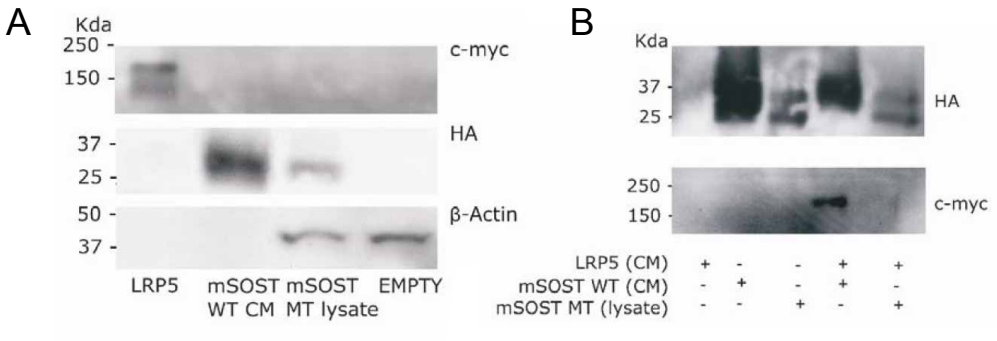

Figure 4. Impaired binding of MT sclerostin to LRP5. A) Total cell lysates and CM from HEK293T cells transfected with WT or MT SOST were analyzed for the expression of HA-tagged sclerostin by immunoblotting using HA antibodies. Expression of LRP5-myc protein in CM was evaluated by immunoblotting with cmyc antibodies. A negative control (empty pcDNA3.1) was included in both immunoblotting experiments. Equal protein loading was confirmed by immunoblotting of total cell lysates for ß-actin. B) Mixtures of CM containing truncated WT-LRP5-myc and either CM containing WT-sclerostin-HA (lane 4) or cell lysates containing MT-sclerostin-HA (lane 5) were immunoprecipitated using EZ-view™ Red Anti-HA affinity gels. Cells that were transfected only with LRP5myc (lane 1) or WT and MT SOST-HA expression vectors (lane 2-3) were used as controls. Immunodetection of HA-immunoprecipitated protein was performed with both anti-HA and anti-myc. From lane 4 and 5 it is clear that WT but not MT sclerostin-HA was able to precipitate LRP5-myc.

Discussion

The clinical and radiological features of patients with SCL are thought to be due to complete absence of sclerostin resulting from loss-of-function mutations in the *SOST* gene. These include both nonsense mutations and splice site mutations [20-22]. In this study, we found for the first time a missense mutation in the *SOST* gene causing a cysteine to arginine amino acid substitution at position 167. The pathogenicity of this genetic variant was demonstrated by the cosegregation of the mutation with the disease in the, albeit small, Turkish family and the absence of the variant in 160 chromosomes of 80 control subjects of a matched ethnic background.

The nature of the mutation is strongly indicative for a pathogenic mutation, since the amino acid substitution results in the loss of a cysteine residue. Alignment of homologous cDNA and protein sequences using CLUSTALW (http://www.ebi.ac.uk/Tools/clustalw2/index.html) showed that the affected cysteine is highly conserved in multiple species (data not shown). Moreover, this cysteine is the last of six cysteines forming the characteristic cystine-knot motif (residues 80-167) [43]. Furthermore, the cysteine to arginine substitution implies a change from an uncharged polar amino acid into a basic amino acid. We tested the putative consequences of this substitution in several software programs, such as Polyphen and SIFT [44, 45]. These programs sort intolerant from tolerant amino acid substitutions, principally on the basis of sequence-homology. Polyphen also includes a search for structural parameters to predict whether an amino acid substitution in a protein has a possible phenotypic effect. According to both programs, the mutation is damaging with a high probability.

Cysteine residues are characterized by thiol-groups that can form disulfide bonds, covalent crosslinks between cysteine side chains that play an important role in the rate and efficiency of protein folding and most importantly in the stability of folded proteins. Some disulfide bonds have been shown to be indispensable for efficient secretion by promoting the production of more compact folded intermediates [46]. Removal of disulfides by site-directed mutagenesis has been demonstrated to be sufficient to cause misfolding, aggregation and impaired secretion of several proteins [47-53].

With regard to the p.Cys167Arg mutation in the *SOST* gene, we used NMR structure analysis of mouse sclerostin to predict the possible influence on the

sclerostin fold. Due to the architecture of the cystine-knot motif three peptide loops emanate from the cystine-knot, two of which run in the same direction (and form the so-called Finger 1 and 2), whereas the third emanates into the opposite direction. Finger 1 and 2 of the WT sclerostin are well defined forming two two-stranded anti-parallel ß-sheets, whereas the third loop is highly flexible and disordered (Supplementary Figure 2A) [54, 55]. A zoom into the cystine-knot motif showed that it is rather loosely packed, with amino acid residues between the cysteine residues pointing towards the solvent, indicating that the cystine-knot of sclerostin exhibits partly elevated flexibility (Supplementary Figure 2B). Simulations in silico suggested that mutating cysteine 167 (equivalent to cysteine 142 of the mature protein) to arginine not only disrupts the outer disulfide bond present in the cystine-knot motif (Supplementary Figure 2C) but also requires conformational changes of the lower loop segment due to the increased spatial requirements of the larger arginine side chain. This will lead to global misfolding due to a decreased stability of the cystine-knot motif and the presence of an accessible reactive thiol-group at the protein surface as one cysteine residue remains unpaired. Even if a global misfolding does not occur, the large space requirements of the arginine side chain will lead to a further disorder of the loop segment, which has been proposed to be important for the activity of sclerostin by mapping the binding site of a neutralizing antibody to the tip of the loop segment [54]. Molecular dynamics simulation indeed showed a local unfolding of the remaining cysteine network, as the side chain of arginine introduced at position 167 (for mature sclerostin residue numbering is not accounting for the 25 residue signal peptide: Cys167 corresponds to Cys142) points towards the interior of the former cystine-knot requiring an opening of the ring in order to avoid steric clashes between the bulky side chain of the introduced arginine and surrounding residues like Cys109, Gly107 and Ser106. This rearrangement is complemented by conformational changes in the amino terminus, as the former packing has to be relieved to create enough space for Arg167. In addition, loss of the disulfide bond between Cys109 and Cys167 (now Arg167) enhances conformational variability in the loop segment since the few hydrophobic interactions between the antiparallel peptide segments of the loop are further weakened.

This in silico modeling suggests that loss of this crucial cysteine may indeed result in impaired folding and hence be responsible for retention of the mutant

protein in the ER. This is normally followed by degradation through delivery to the 26S proteasome in the cytoplasm or by lysosomal degradation by autophagy. The latter mechanism is especially used for misfolded proteins that aggregate in the secretory pathway or in the cytosol [56, 57]. Using subcellular localization experiments, we were able to show that MT sclerostin indeed does not exit the ER, explaining the decreased extracellular levels of MT sclerostin compared to WT found by immunoblotting and electrochemiluminescence. In addition, in reporter assays MT sclerostin was found to have strongly decreased antagonistic activity on Wnt signaling. Using co-IP experiments, we demonstrated that also the binding affinity of MT sclerostin for LRP5, which is required for its antagonist activity, is decreased. *In vivo*, these effects resulted in a complete loss of function of sclerostin reflected by a phenotype that is highly similar to that of previously reported patients with SCL. In the same way, loss-of-function mutations derived from folding problems in a variety of proteins with different activities, lead to retention of mutated proteins in the ER and their consequent degradation. This mechanism lies at the basis of a large number of ER-derived diseases, reviewed by Aridor et al [58]. In addition to this loss-of-function, increased levels of ER stress, known as unfolded protein response (UPR) (i.e. induction of inflammatory responses or cellular apoptosis), due to inability of the ER to efficiently dispose of the mutant protein, can contribute substantially to disease pathogenesis [58, 59]. It has been reported that strongly secretory cells (and maybe also the osteocyte) are extremely susceptible to this UPR, which often results in a pathogenic outcome [59]. Since we did not perform experiments to further investigate this disease mechanism, our data can not exclude the possibility that this mechanism additionally contributes to the phenotype in this family.

In conclusion, the present work describes here the first missense mutation in the *SOST* gene encoding sclerostin in a patient with SCL. This missense mutation involves one of the cysteine residues of the cystine-knot motif of sclerostin. The mutation has a devastating effect on the biological function of sclerostin by reducing extracellular sclerostin levels as well as the binding capacity of sclerostin to LRP5 and, thereby, its antagonistic activity on canonical Wnt signaling. It is possible that ER stress and UPR, as a consequence of the inability of the ER to efficiently dispose of the mutant protein, also contribute to the disease phenotype.

Acknowledgments

This work was supported by the European Commission [HEALTH-F2-2008-201099, TALOS]; and by grants from the 'Fonds voor Wetenschappelijk Onderzoek' [FWO, G.0117.06], from the Special Research Funds (BOF TOP and NOI) of the University of Antwerp, all to W.V.H.. Additional support was provided by Senternovem/IOP Genomics (IGE07001A).

References

1. Gueguen R, Jouanny P, Guillemin F, Kuntz C, Pourel J, Siest G. Segregation analysis and variance components analysis of bone mineral density in healthy families. J Bone Miner Res 1995;10:2017-22.

2. Krall EA, Dawson-Hughes B. Heritable and life-style determinants of bone mineral density. J Bone Miner Res 1993;8:1-9.

3. Balemans W, Van Wesenbeeck L, Van Hul W. A clinical and molecular overview of the human osteopetroses. Calcif Tissue Int 2005;77:263-74.

4. Johnson ML, Harnish K, Nusse R, Van Hul W. LRP5 and Wnt signaling: a union made for bone. J Bone Miner Res 2004;19:1749-57.

5. Beighton P, Barnard A, Hamersma H, van der Wouden A. The syndromic status of sclerosteosis and Van Buchem disease. Clin Genet 1984;25:175-81.

6. Beighton P, Davidson J, Durr L, Hamersma H. Sclerosteosis - an autosomal recessive disorder. Clin Genet 1977;11:1-7.

7. Beighton P, Durr L, Hamersma H. The clinical features of sclerosteosis. A review of the manifestations in twenty-five affected individuals. Ann Intern Med 1976;84:393-7.

8. Hamersma H, Gardner J, Beighton P. The natural history of sclerosteosis. Clin Genet 2003;63:192-7.

9. Freire de Paes-Alves A, Cardoso L, Rabelo MM. Sclerosteosis: a marker for Dutch ancestry? Rev Brasil Genet 1982;4:825-34.

10. Bueno M, Olivan G, Jimenez A, Garagorri JM, Sarria A, Bueno AL *et al.* Sclerosteosis in a Spanish male: first report in a person of Mediterranean origin. J Med Genet 1994;31:976-7.

11. Kelley CH, Lawlah JW. Albers-Schonberg disease; a family survey. Radiology 1946;47:507-13.

12. Higinbotham NL, Alexander SF. Osteopetrosis: four cases in one family. Am J Surgery 1941;53:444-54.

13. Pietruschka G. [Further information on marble bones (Albers-Schonberg disease) with remarks on differential diagnosis]. Klin Monbl Augenheilkd Augenarztl Fortbild 1958;132:509-25.

14. Stein SA, Witkop C, Hill SC, Fallon MD, Viernstein L, Gucer G *et al.* Sclerosteosis: neurogenetic and pathophysiologic analysis of an American kinship. Neurology 1983;33:267-77.

15. Sugiura Y, Yasuhara T. Sclerosteosis. A case report. J Bone Joint Surg Am 1975;57:273-7.

16. Tacconi P, Ferrigno P, Cocco L, Cannas A, Tamburini G, Bergonzi P *et al.* Sclerosteosis: report of a case in a black African man. Clin Genet 1998;53:497-501.

17. Dixon JM, Cull RE, Gamble P. Two cases of Van Buchem's disease. J Neurol Neurosurg Psychiatry 1982;45:913-8.

18. Balemans W, van den Ende J, Freire de Paes-Alves A, Dikkers FG, Willems PJ, Vanhoenacker F *et al.* Localization of the gene for sclerosteosis to the Van Buchem disease-gene region on chromosome 17q12-q21. Am J Hum Genet 1999;64:1661-9.

19. Van Hul W, Balemans W, Van Hul E, Dikkers FG, Obee H, Stokroos RJ *et al.* Van Buchem disease (hyperostosis corticalis generalisata) maps to chromosome 17q12-q21. Am J Hum Genet 1998;62:391-9.

20. Balemans W, Ebeling M, Patel N, van Hul E, Olson P, Dioszegi M *et al.* Increased bone density in sclerosteosis is due to the deficiency of a novel secreted protein (SOST). Hum Mol Genet 2001;10:537-43.

21. Brunkow ME, Gardner JC, Van Ness J, Paeper BW, Kovacevich BR, Proll S *et al.* Bone dysplasia sclerosteosis results from loss of the *SOST* gene product, a novel cystine knot-containing protein. Am J Hum Genet 2001;68:577-89.

22. Balemans W, Cleiren E, Siebers U, Horst J, van Hul W. A generalized skeletal hyperostosis in two siblings caused by a novel mutation in the *SOST* gene. Bone 2005;36:943-7.

23. Balemans W, Patel N, Ebeling M, Van Hul E, Wuyts W, Lacza C *et al.* Identification of a 52 kb deletion downstream of the *SOST* gene in patients with Van Buchem disease. J Med Genet 2002;39:91-7.

24. Staehling-Hampton K, Proll S, Paeper BW, Zhao L, Charmley P, Brown A *et al.* A 52-kb deletion in the SOST-MEOX1 intergenic region on 17q12-q21 is associated with Van Buchem disease in the Dutch population. Am J Med Genet 2002;110:144-52.

25. van Bezooijen RL, Bronckers AL, Gortzak RA, Hogendoorn PC, Wee-Pals L, Balemans W *et al.* Sclerostin in mineralized matrices and Van Buchem disease. J Dent Res 2009;88:569-74.

26. van Bezooijen RL, Roelen BA, Visser A, van der Wee-Pals, de Wilt E, Karperien M *et al.* Sclerostin is an osteocyte-expressed negative regulator of bone formation, but not a classical BMP antagonist. J Exp Med 2004;199:805-14.

27. Hill SC, Stein SA, Dwyer A, Altman J, Dorwart R, Doppman J. Cranial CT findings in sclerosteosis. AJNR Am J Neuroradiol 1986;7:505-11.

28. van Bezooijen RL, ten Dijke P, Papapoulos SE, Löwik CWGM. SOST/sclerostin, an osteocyte-derived negative regulator of bone formation. Cytokine Growth Factor Rev 2005;16:319-27.

29. Li X, Ominsky MS, Niu QT, Sun N, Daugherty B, D'Agostin D *et al.* Targeted deletion of the sclerostin gene in mice results in increased bone formation and bone strength. J Bone Miner Res 2008;23:860-9.

30. Sutherland MK, Geoghegan JC, Yu C, Turcott E, Skonier JE, Winkler DG *et al.* Sclerostin promotes the apoptosis of human osteoblastic cells: a novel regulation of bone formation. Bone 2004;35:828-35.

31. van Bezooijen RL, Svensson JP, Eefting D, Visser A, van der Horst G, Karperien M *et al.* Wnt but not BMP signaling is involved in the inhibitory action of sclerostin on BMP-stimulated bone formation. J Bone Miner Res 2007;22:19-28.

32. Winkler DG, Sutherland MK, Geoghegan JC, Yu C, Hayes T, Skonier JE *et al.* Osteocyte control of bone formation via sclerostin, a novel BMP antagonist. EMBO J 2003;22:6267-76.

33. Li X, Zhang Y, Kang H, Liu W, Liu P, Zhang J *et al.* Sclerostin binds to LRP5/6 and antagonizes canonical Wnt signaling. J Biol Chem 2005;280:19883-7.

34. Semenov M, Tamai K, He X. SOST is a ligand for LRP5/LRP6 and a Wnt signaling inhibitor. J Biol Chem 2005;280:26770-5.

35. Boyden LM, Mao J, Belsky J, Mitzner L, Farhi A, Mitnick MA *et al.* High bone density due to a mutation in LDL-receptor-related protein 5. N Engl J Med 2002;346:1513-21.

36. Little RD, Carulli JP, Del Mastro RG, Dupuis J, Osborne M, Folz C *et al.* A mutation in the LDL receptor-related protein 5 gene results in the autosomal dominant high-bone-mass trait. Am J Hum Genet 2002;70:11-9.

37. Van Wesenbeeck L, Cleiren E, Gram J, Beals RK, Benichou O, Scopelliti D *et al.* Six novel missense mutations in the LDL receptor-related protein 5 (LRP5) gene in different conditions with an increased bone density. Am J Hum Genet 2003;72:763-71.

38. Balemans W, Piters E, Cleiren E, Ai M, Van Wesenbeeck L, Warman ML *et al.* The binding between sclerostin and LRP5 is altered by DKK1 and by high-bone mass LRP5 mutations. Calcif Tissue Int 2008;82:445-53.

39. Ellies DL, Viviano B, McCarthy J, Rey JP, Itasaki N, Saunders S *et al.* Bone density ligand, Sclerostin, directly interacts with LRP5 but not LRP5G171V to modulate Wnt activity. J Bone Miner Res 2006;21:1738-49.

40. Semenov MV, He X. LRP5 mutations linked to high bone mass diseases cause reduced LRP5 binding and inhibition by SOST. J Biol Chem 2006;281:38276-84.

41. Piters E, Boudin E, Van Hul W. Wnt signaling: a win for bone. Arch Biochem Biophys 2008;473:112-6.

42. Ellgaard L, Helenius A. Quality control in the endoplasmic reticulum. Nat Rev Mol Cell Biol 2003;4:181-91.

43. Avsian-Kretchmer O, Hsueh AJ. Comparative genomic analysis of the eight-membered ring cystine knot-containing bone morphogenetic protein antagonists. Mol Endocrinol 2004;18:1-12.

44. Ng PC, Henikoff S. SIFT: Predicting amino acid changes that affect protein function. Nucleic Acids Res 2003;31:3812-4.

45. Ramensky V, Bork P, Sunyaev S. Human non-synonymous SNPs: server and survey. Nucleic Acids Res 2002;30:3894-900.

46. Wittrup KD. Disulfide bond formation and eukaryotic secretory productivity. Curr Opin Biotechnol 1995;6:203-8.

47. Bedows E, Norton SE, Huth JR, Suganuma N, Boime I, Ruddon RW. Misfolded human chorionic gonadotropin beta subunits are secreted from transfected Chinese hamster ovary cells. J Biol Chem 1994;269:10574-80.

48. Chen XZ, Shafer AW, Yun JS, Li YS, Wagner TE, Kopchick JJ. Conversion of bovine growth hormone cysteine residues to serine affects secretion by cultured cells and growth rates in transgenic mice. Mol Endocrinol 1992;6:598-606.

49. Omura F, Otsu M, Kikuchi M. Accelerated secretion of human lysozyme with a disulfide bond mutation. Eur J Biochem 1992;205:551-9.

50. Segal MS, Bye JM, Sambrook JF, Gething MJ. Disulfide bond formation during the folding of influenza virus hemagglutinin. J Cell Biol 1992;118:227-44.

51. Shani O, Pines O. The relationship between disulphide bond formation, processing and secretion of lipo-beta-lactamase in yeast. Mol Microbiol 1992;6:189-95.

52. Suganuma N, Matzuk MM, Boime I. Elimination of disulfide bonds affects assembly and secretion of the human chorionic gonadotropin beta subunit. J Biol Chem 1989;264:19302-7.

53. Taniyama Y, Yamamoto Y, Nakao M, Kikuchi M, Ikehara M. Role of disulfide bonds in folding and secretion of human lysozyme in Saccharomyces cerevisiae. Biochem Biophys Res Commun 1988;152:962-7.

54. Veverka V, Henry AJ, Slocombe PM, Ventom A, Mulloy B, Muskett FW *et al.* Characterization of the structural features and interactions of sclerostin: molecular insight into a key regulator of Wnt-mediated bone formation. J Biol Chem 2009;284:10890-900.

55. Weidauer SE, Schmieder P, Beerbaum M, Schmitz W, Oschkinat H, Mueller TD. NMR structure of the Wnt modulator protein Sclerostin. Biochem Biophys Res Commun 2009;380:160-5.

56. Klionsky DJ. Autophagy: from phenomenology to molecular understanding in less than a decade. Nat Rev Mol Cell Biol 2007;8:931-7.

57. Nakatsukasa K, Brodsky JL. The recognition and retrotranslocation of misfolded proteins from the endoplasmic reticulum. Traffic 2008;9:861-70.

58. Aridor M. Visiting the ER: the endoplasmic reticulum as a target for therapeutics in traffic related diseases. Adv Drug Deliv Rev 2007;59:759-81.

59. Boot-Handford RP, Briggs MD. The unfolded protein response and its relevance to connective tissue diseases. Cell Tissue Res 2010;339:197-211.

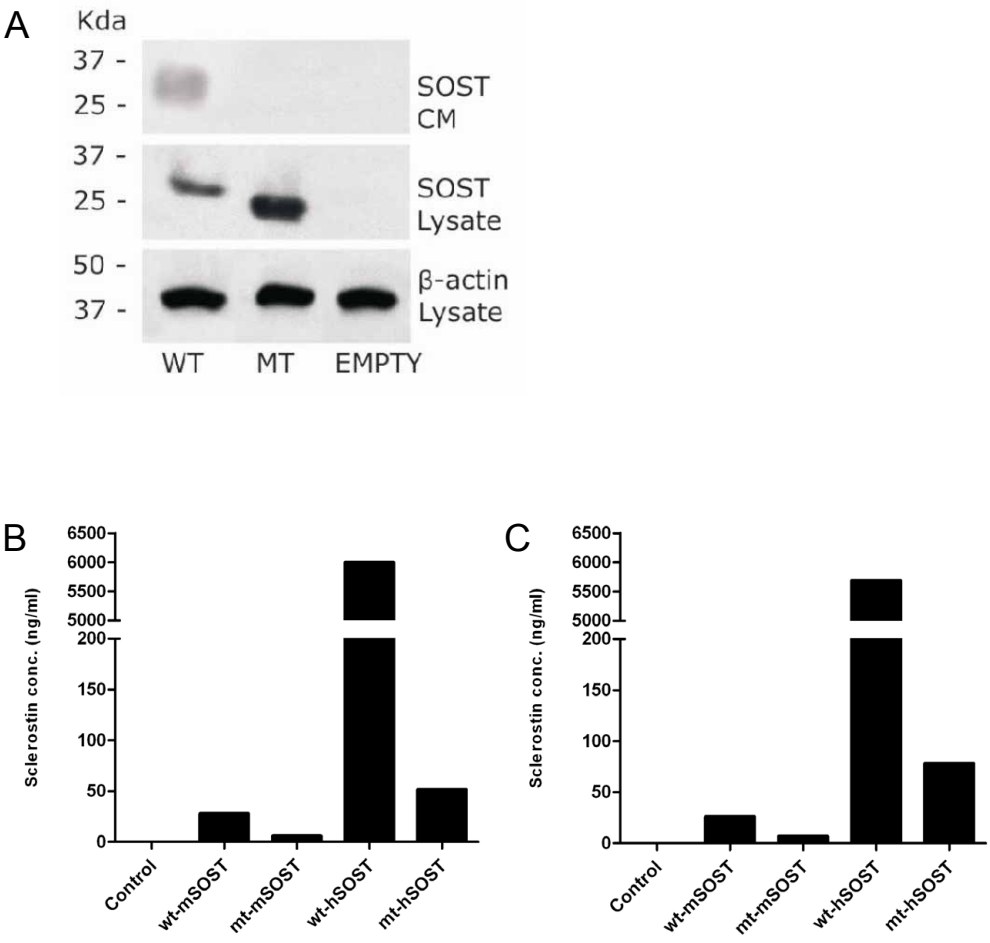

Supplementary Figure 1. Decreased intra- and extracellular levels of MT sclerostin. A) Total cell lysates and CM from HEK293T cells transfected with WT or MT SOST or empty vector were analyzed for the expression of HA-tagged sclerostin by immunoblotting using an HA antibody. Equal protein loading was confirmed by immunoblotting of total cell lysates for ß-actin. One representative experiment of three independent immunoblotting experiments is depicted. B) Quantitative expression analysis of sclerostin in cell lysates of HEK293T cells transfected with WT and MT constructs of both mouse and human SOST or an empty control vector using the MULTI-ARRAY® Human sclerostin assay (MSD). Sclerostin levels were corrected for SOST mRNA expression levels for each of the plasmids determined by RT-PCR analysis. C) Same in CM of transfected HEK293T cells.

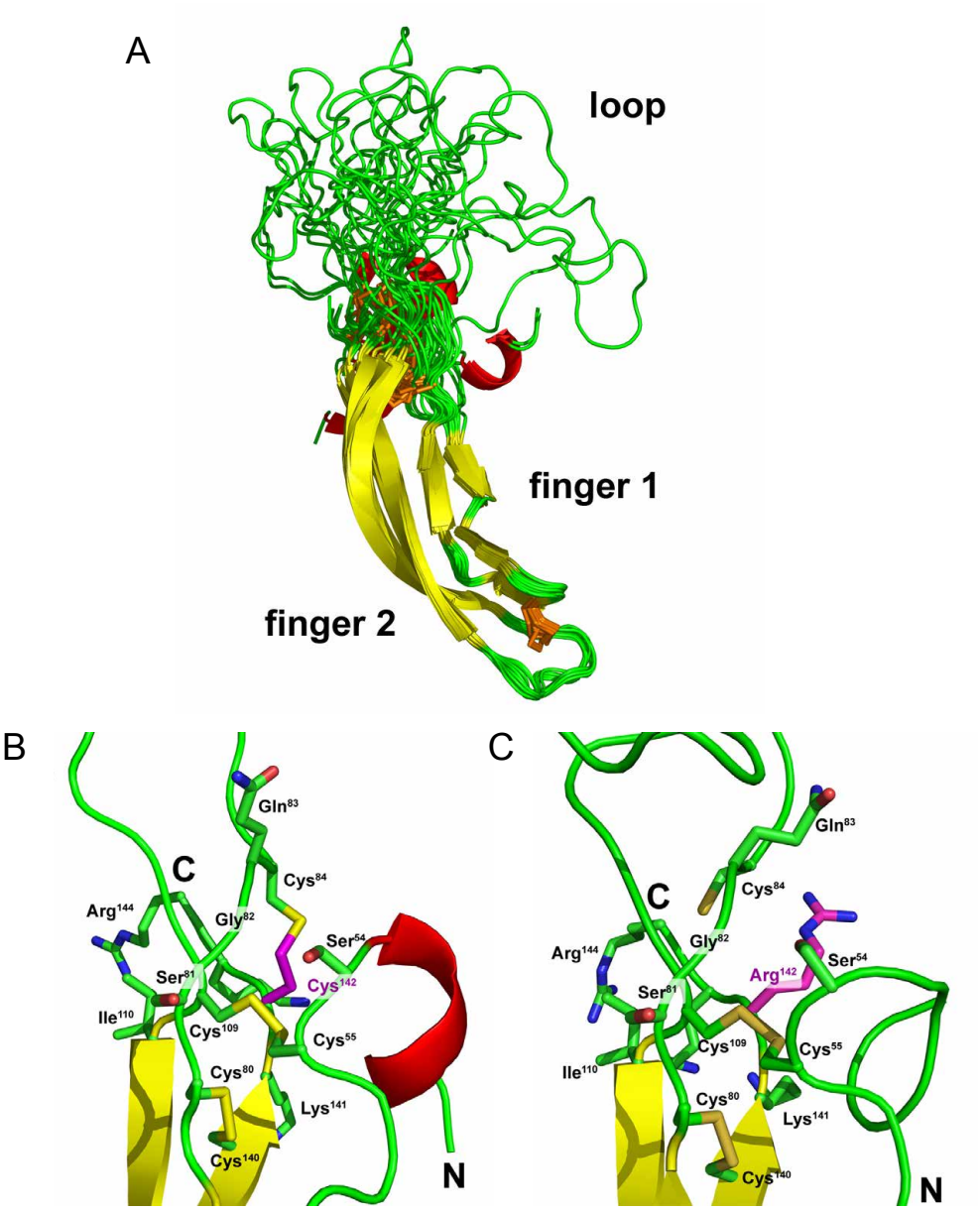

Supplementary Figure 2. Effect of the mutating cysteine 167 to arginine on the NMR structure of sclerostin. A) Ribbon representation of the NMR structure ensemble of mouse sclerostin (residues Lys73 to Arg169 is shown, residue numbering includes the 25 residue signal peptide, PDB entry 2KD3). The secondary structure elements are indicated in yellow (ß-strand), red (a-helix) and green (coil). The overlay of the 15 NMR structures of the ensemble shows that finger 1 and 2 are well defined, whereas the loop is highly flexible and disordered. B) Detail of the cystine-knot of sclerostin. The cystine-knot is rather loosely packed, with amino acid residues between the cysteine residues pointing towards the solvent, indicating that the cystine-knot of sclerostin is flexible in part. The cysteine residue, which is mutated in the patient, is colored in magenta, numbering is according to full-length sclerostin protein starting with residue 1. C) Same region displayed for MT mouse sclerostin variant. Mutating cysteine 167 to arginine disrupts the outer disulfide bond present in the cystine-knot motif.